JACS Au
AN OPEN ACCESS JOURNAL OF THE AMERICAN CHEMICAL SOCIETY

pubs.acs.org/jacsau

Article

Aggregation-Induced Emission Metallocuboctahedra for White Light Devices

Zhe Zhang,[⊥] Yan Huang,[⊥] Qixia Bai,[⊥] Tun Wu, Zhiyuan Jiang, Haoyue Su, Yingxin Zong, Ming Wang, Pei-Yang Su,* Ting-Zheng Xie,* and Pingshan Wang*

Cite This: *JACS Au* 2022, 2, 2809−2820

Read Online

ACCESS | Metrics & More | Article Recommendations | Supporting Information

ABSTRACT: Materials for organic light-emitting devices which exhibit superior emission properties in both the solution and solid states with a high fluorescence quantum yield have been extensively sought after. Herein, two metallocages, **S1** and **S2**, were constructed, and both showed typical aggregation-induced emission (AIE) features with intense yellow fluorescence. By adding blue-emissive 9,10-dimethylanthracene, pure white light emission can be produced in the solution of **S1** and **S2**. Furthermore, due to the remarkable AIE feature and good fluorescence quantum yield in the solid state, metallocages are highly emissive in the solid state and can be utilized to coat blue LED bulbs or integrate with blue-emitting chips to obtain white light. This study advances the usage of metallocages as practical solid-state fluorescent materials and provides a fresh perspective on highly emissive AIE materials.

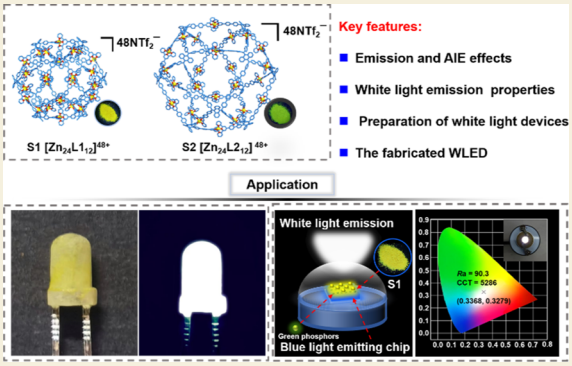

KEYWORDS: *aggregation-induced emission, metallocages, self-assembly, white light emission*

INTRODUCTION

In recent years, luminescent materials have gained considerable research efforts owing to their outstanding properties and wide range of applications in sensing,[1−4] cell imaging,[5−7] encrypted information,[8,9] and so forth.[10−12] In general, emission efficiencies of most luminophores tend to be weakened or quenched by aggregation-caused quenching (ACQ).[13] Fortunately, the aggregation-induced fluorescence enhancement phenomenon (AIE)[14−17] proposed by Tang et al. had solved this problem. From then on, coupled with the low cost, lightweight, and ease of manufacturing thin films[18] of organic light-emitting materials, research based on this topic[19−22] has developed rapidly. Meanwhile, bottom-up coordination-driven self-assembly has been proven to be a powerful tool for building supramolecular structures ranging from basic two-dimensional macrocycles[23−31] to increasingly complex three-dimensional cages,[32−39] which has various applications in catalysis,[40−43] host−guest recognition,[44−46] molecular separation,[47,48] and so forth.[49−52] Recently, due to the presence of ligand-induced emission, numerous AIE-based luminescent supramolecular materials have also been constructed by incorporating tetraphenylethylene (TPE) and other typical fluorescent groups[53,54] into metal-organic frameworks,[55−58] metal macrocycles,[59−62] and metallocages.[63−67] Specifically, among the luminescent coordination systems, obtaining a supramolecular structure-based white light emission (WLE) system[68−73] is a goal pursued by supramolecular chemists. For example, Zhang et al. reported a solid-state fluorescent material based on a TPE-multicomponent emissive metal cage and successfully achieved WLE.[74] Nitschke et al. achieved WLE from an M_4L_6 supramolecular cage by introducing a series of fluorophores.[75] However, regardless of solution or solid emission, they were both achieved through anchoring AIE emitting groups to metals within rigid scaffolds or by direct introduction of ligands. In contrast, the realization of supramolecular structures with AIE effects from ligands with ACQ has been rarely explored, and the simultaneous realization of solution and solid WLE in supramolecular systems still presents a challenging endeavor.

Herein, we reported two terpyridine-based tunable luminescent cuboctahedral metallocages **S1** and **S2** which have good solution- and solid-state luminescence properties. **S1** and **S2** are generated by the coordination-driven self-assembly of two dihydroanthracenyl tetrakisterpyridine organic ligands and zinc ions. Interestingly, **S1** and **S2** exhibited faint emission in diluted dimethylformamide (DMF) solution but had good AIE properties with the addition of poor solvents. Furthermore, due to their yellow fluorescence emission (λ_{em} = 550 nm), WLE of these cages in the solution state was performed by

Received: October 17, 2022
Revised: November 19, 2022
Accepted: November 22, 2022
Published: December 9, 2022

https://doi.org/10.1021/jacsau.2c00568
JACS Au 2022, 2, 2809−2820

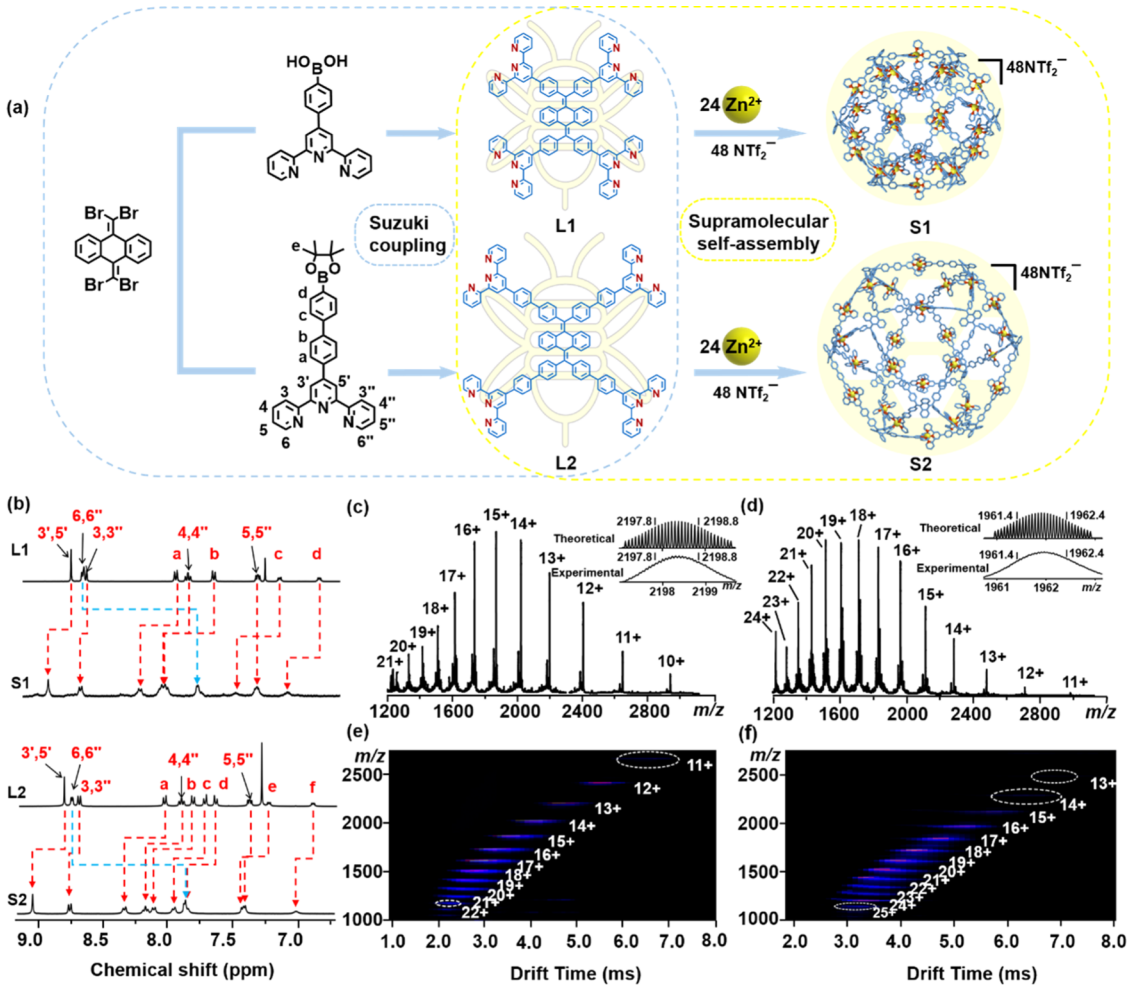

Figure 1. (a) Synthesis of ligands **L1** and **L2** and of supramolecules **S1** and **S2**; (b) ^{1}H NMR spectra of **L1**, **L2**, **S1**, and **S2** (400 MHz, 298 K, $CDCl_3$ for ligands and CD_3CN for supramolecules); (c,e) ESI-MS and TWIM-MS spectra of **S1**; (d,f) ESI-MS and TWIM-MS spectra of **S2**.

Scheme 1. Fabrication of White Light Devices Using the Metallocages S1 and S2 with Superb AIE Characteristics

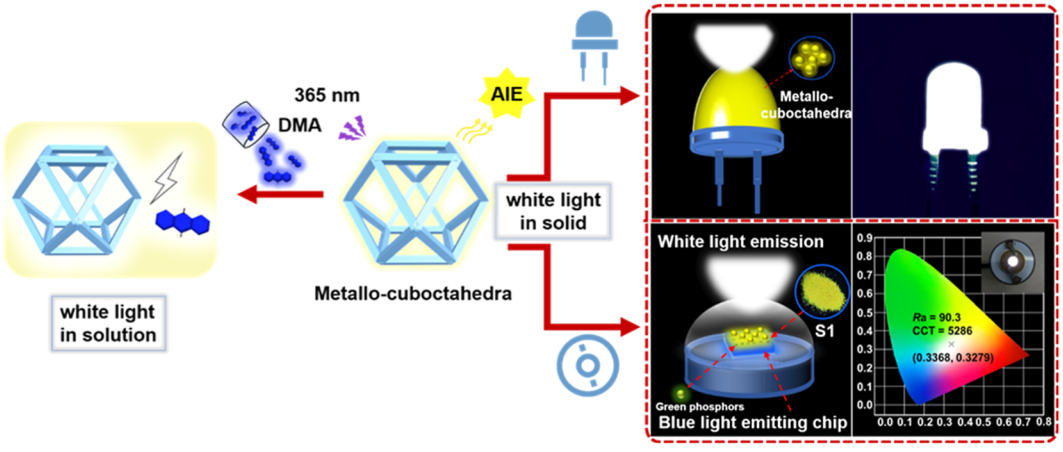

introducing deep-blue emissive (CIE < 0.10) molecules [9,10-dimethylanthracene (DMA)]. Due to the restricted molecular motion after coordination, the metallocages have a better emission intensity in the solid state, combined with their good solubility, they can be easily coated on the surface of blue LED bulbs to construct white LED bulbs. Further, a white LED element with stable color output and stable light conversion was constructed with CIE coordinates of (0.3368, 0.3279), color rendering index (CRI, *Ra*) of 90.3, and CCT of 5286 K by integrating with the blue-emitting chip (Scheme S1). The exploration of such luminescent metallocages could provide a novel method for the preparation of tunable and highly emissive luminescent materials.

https://doi.org/10.1021/jacsau.2c00568
JACS Au 2022, 2, 2809−2820

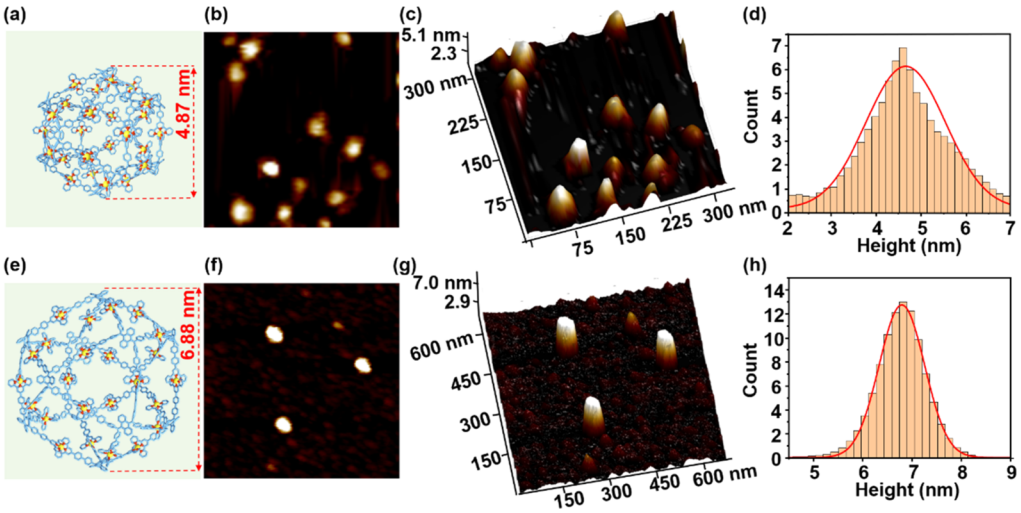

Figure 2. AFM images of **S1** and **S2**. (a,e) Representative energy-minimized molecular modeling of **S1** and **S2**; (b,c) 2D and 3D AFM images of **S1**; (d) height statistical histogram of AFM for 100 particles of **S1**. (f,g) 2D and 3D AFM images of **S2**; (h) height statistical histogram of AFM for 100 particles of **S2**.

RESULTS AND DISCUSSION

Synthesis and Characterization of Metallocages S1 and S2

L1 and **L2** were synthesized by a four-fold Suzuki coupling reaction using dihydro anthracenyl tetrabromide[76] **1** and intermediates **2** or **4** in decent yields as shown in Figure 1a.The ligands (Scheme 1) were characterized by NMR spectroscopy and high-resolution mass spectrometry, including ^{1}H, ^{13}C, COSY, NOESY, and electrospray ionization-mass spectrometry (ESI-MS) (Figures S7−S20). Subsequently, the ligands were assembled with $Zn(NTf_2)_2$ at a precise stoichiometric ratio of 1:2 in a $CHCl_3$/MeOH (1:1, v/v) solution to form the metallocages **S1** and **S2** in 96% yield, separately. Figure 1b shows the ^{1}H NMR spectra of ligands and their corresponding complexes. Take **S1**, for example, a dramatic upfield shift for the $H^{6,6''}$ signal from 8.72 to 7.71 ppm ($\Delta\delta$ = 1.01) (Figure 1b) was indicative of terpyridine complex formation. The distinct and sharp signals strongly suggested a highly symmetric and discrete structure. In addition, all the NMR resonance signals of the metallocages were clearly assigned by COSY and NOESY (Figures S25, S26, S32 and S33), indicating the formation of metallocages. The DOSY experiments provide more structural information on **S1** and **S2** (Figures S27 and S34). All spectra showed a narrow signal band indicating that no other structures were present in the self-assembly, with diffusion coefficients (D) of around $10^{-9.68}$ and $10^{-9.80}$ m^2 s^{-1} corresponding to **S1** and **S2**, respectively. The radii of the spherical complexes were calculated to be 2.82 and 3.72 nm according to the Stokes−Einstein equations, which are slightly larger than the expected values from molecular modeling (Figures 2a,e and 3k,r). It was that the difference between the molecular modeling and the results of DOSY comes from the attached anions around the cages.

Additional support for **S1** and **S2** was provided by ESI-MS coupled with traveling-wave ion mobility MS (TWIM-MS) experiments. Figure 1c shows one dominant set of peaks with continuous charge states from 11+ to 22+, corresponding to successively losing NTf_2^- counterions. As expected, the average measured molecular mass of **S1** is 32219.88 Da, corresponding to the combination of 12 ligands, 24 zinc ions, and 48 anions. The m/z values along with isotopic patterns of each charge state matched well with the corresponding calculated values (Figure S3). TWIM-MS results[77] (Figure 1e) show a range of signals at each charge state (m/z) with a narrow distribution, clearly indicating that no other isomers or conformers are present for **S1**. Similarly, the formation of **S2** is demonstrated using ESI-MS and TWIM-MS (Figure 1d,f). The gMS^2 experiments were performed by collision-induced dissociation for 15+ ions of **S1** with m/z of 1868.2. There was no pronounced fragmentation peak below 36 V, and when the voltage reached 54 V, the complex ions wholly dissociated, exhibiting high stability (Figure S5). The stability of **S2** was examined under the same testing conditions, which showed slightly weaker stability than **S1** (Figure S6).

Transmission electron microscopy (TEM) and atomic force microscopy (AFM) were employed to further confirm the height and dimensions of cuboctahedral cages **S1** and **S2**. In the TEM images (Figures 3l,s and S36), the uniformly distributed individual dot patterns of **S1** and **S2** were observed. The size information obtained from the TEM is comparable to the theoretical diameters of **S1** and **S2** of 4.9 and 6.9 nm, respectively, which were obtained from the optimized molecular model. In the AFM images, the individual dots were observed to have the height of a single molecule, which is consistent with the molecular modeling (Figure 2b,f). It is also proved by the height statistics histogram that most of the points have a height of 5.0 and 7.0 nm (Figure 2c,d,g and h). The crystals were successfully got by slow diffusion of ethyl acetate into the DMF solution of **S1** or **S2**, but unfortunately, the final perfect crystal structure was not attained due to the large volume of the unit cell and a large number of disordered counter ions and wrapping of solvent molecules (Figures S1 and S2).

Emission and AIE Effects of S1 and S2

The photophysical properties of the complexes were investigated by UV−vis (Figure S37) and fluorescence spectrometry. Compared with ligands **L1** and **L2**, which have typical aggregation-caused quenching effects (ACQ) (Figures S39 and S40), the complexes **S1** and **S2** showed high emission efficiency in the aggregated state due to the restriction of intramolecular rotation (RIR) caused by the formation of a

https://doi.org/10.1021/jacsau.2c00568
JACS Au 2022, 2, 2809−2820

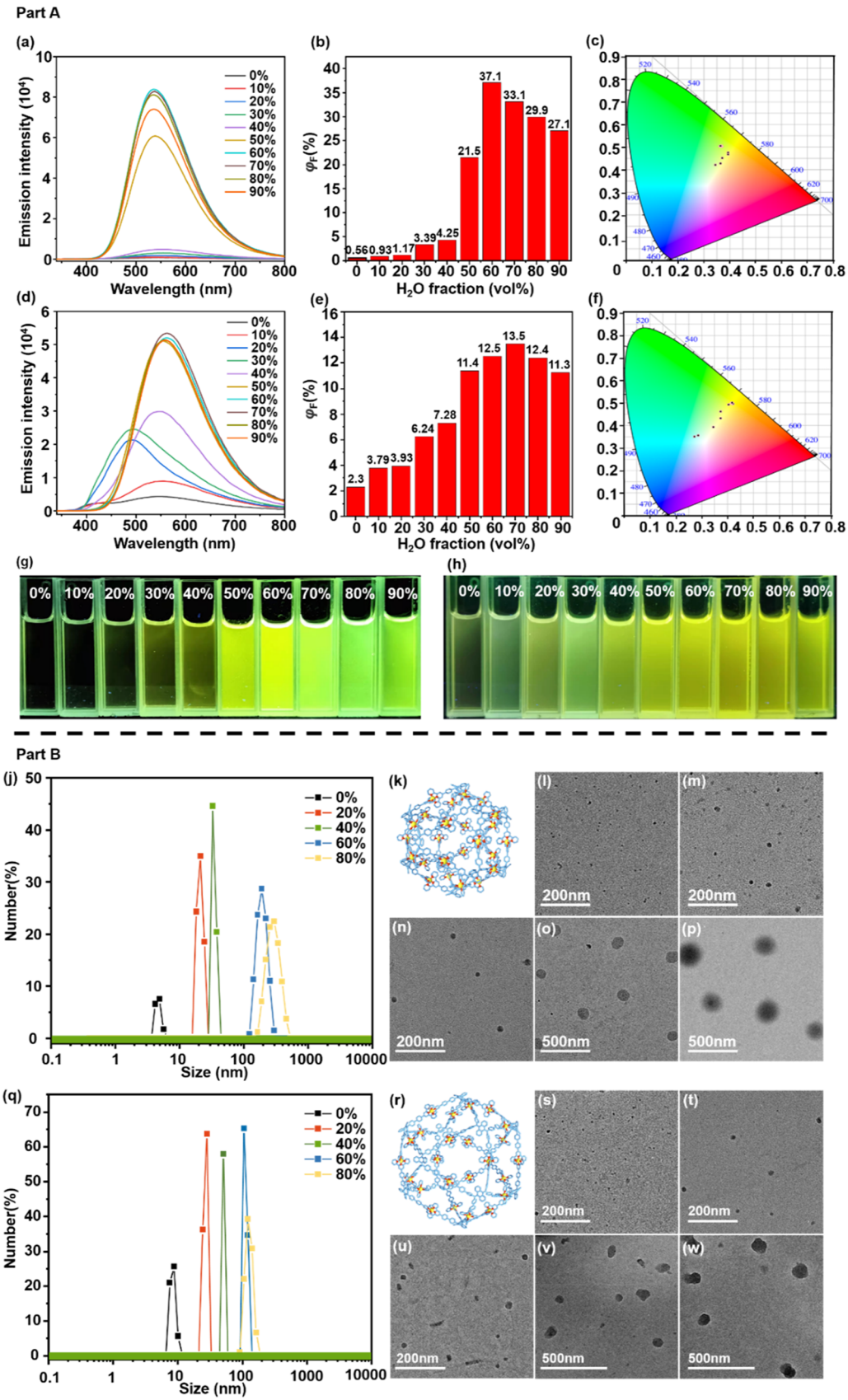

Figure 3. Part A: AIE of **S1** and **S2**. (a,d) Fluorescence spectrum (λ_{ex} = 326 nm, c = 1.0 μM), (b,e) quantum yields, (c,f) CIE 1931 chromaticity diagram (the crosses signify the luminescent color coordinates), and (g,h) photographs of **S1** and **S2** in DMF/H_2O with various fractions. Part B: TEM images and DLS of **S1** and **S2** aggregates. (j,q) Size distributions of **S1** and **S2** in DMF/H_2O mixtures determined by DLS (percentages in the graphs are poor solvent contents); (k,r) representative energy-minimized molecular modeling of **S1** and **S2**; TEM images of **S1** and **S2** in DMF/H_2O mixtures containing (l,s) 0%, (m,t) 20%, (n,u) 40%, (o,v) 60%, and (p,w) 80% H_2O.

https://doi.org/10.1021/jacsau.2c00568
JACS Au 2022, 2, 2809−2820

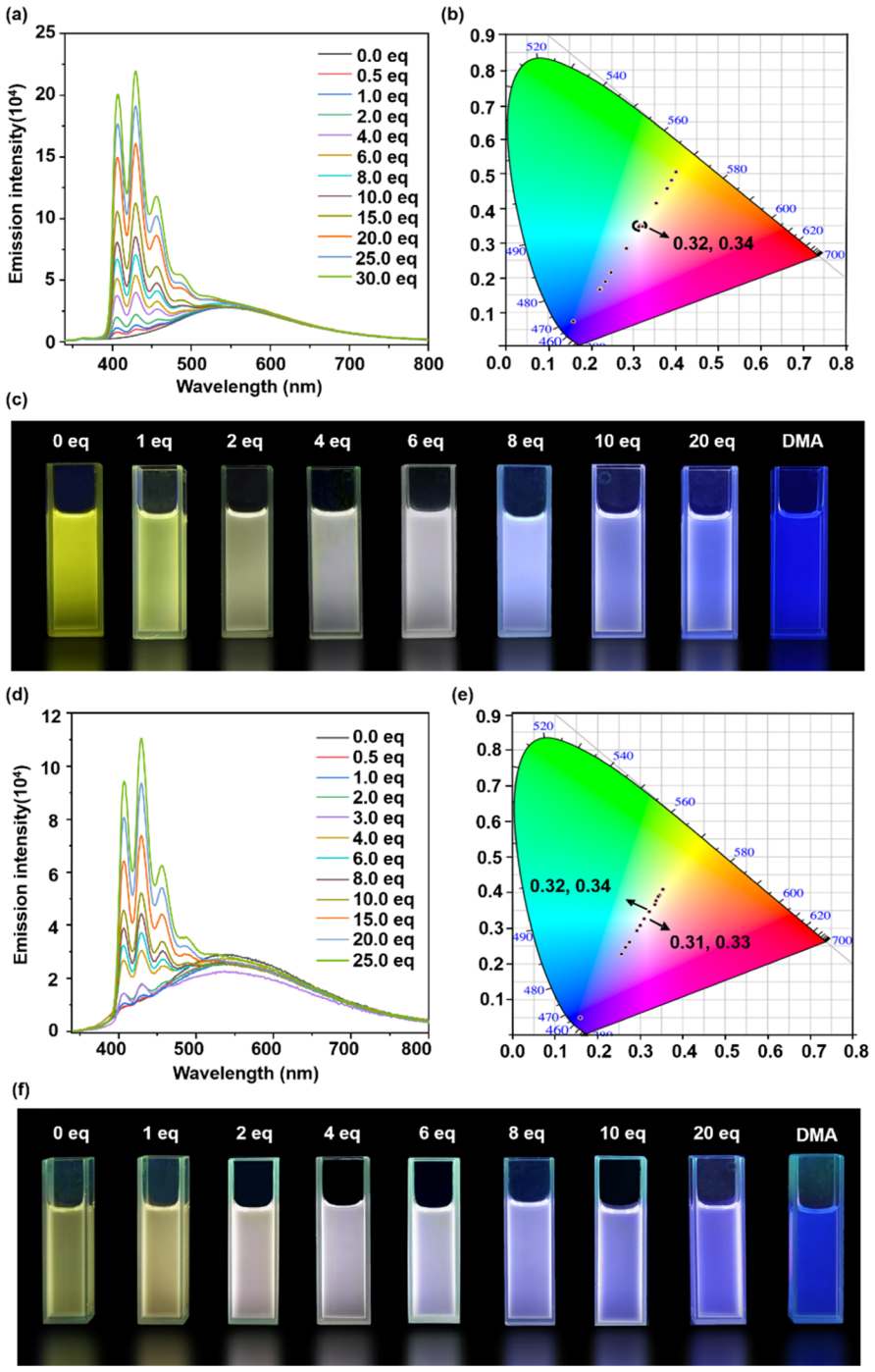

Figure 4. WLE of **S1** and **S2**. (a,d) Fluorescence spectrum (λ_{ex} = 326 nm and $c = 1.0 \times 10^{-5}$ M), (b,e) CIE 1931 chromaticity diagram (crosses signify luminescent color coordinates), and (c,f) photographs of **S1** and **S2** in DMF with different equivalents of DMA.

coordination cage.[78−81] In a dilute solution of DMF, **S1** showed only a weak emission centered at 550 nm (Figure 3a,g), which was attributed to the allowed metal−ligand charge transfer transition.[82] When the poor solvent H_2O fractions were increased from 10 to 60%, the emission intensity at 515 nm was induced and greatly increased, that is, Φ_F intensity increased from 0.5% for 0% H_2O to 37.1% for 60% H_2O, indicating an aggregation-induced fluorescence phenomenon triggered by the RIR effect. When the water content exceeds 60%, the quantum yield of **S1** decreases slightly due to the increased intermolecular collisions in the aggregated state (Figure 3b,c). **S2** displayed a similar AIE process, with a maximum Φ_F intensity of 13.5 at 70% H_2O (Figure 3e,f,h). With an increased proportion of H_2O to 80%, there is a slight decrease in fluorescence intensity since the tight arrangement of the supramolecules increases the intramolecular collisions, which leads to a loss of energy (Figure 3d,e).

In addition, TEM experiments of the **S1** and **S2** aggregates afforded direct evidence for the formation of the aggregates. As displayed in Figure 3l−p, the images determined by drop-casting the mixture onto a Cu grid for TEM showed that the nano spherical particles formed in the DMF/H_2O mixture. With the addition of poor solvents, the size of **S1** aggregates increased from 6.6 to 120 nm, it can be seen that the average

https://doi.org/10.1021/jacsau.2c00568
JACS Au 2022, 2, 2809−2820

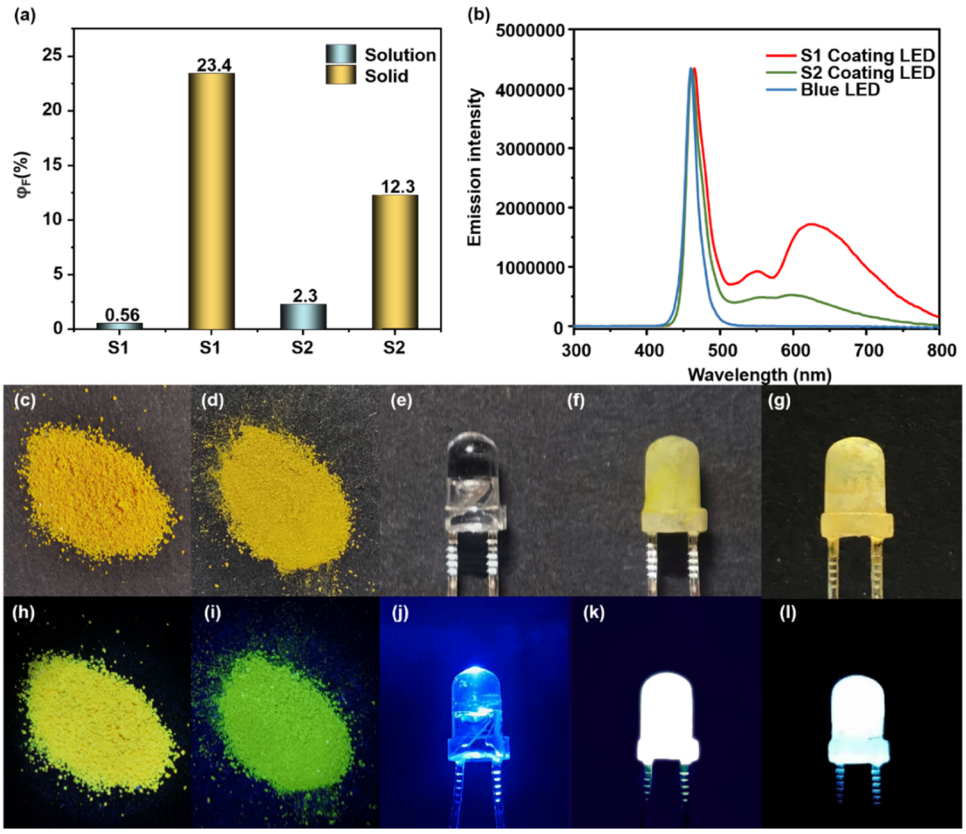

Figure 5. Preparation of solid-state fluorescent and white light devices. (a) Absolute fluorescence quantum yields of **S1** and **S2** in acetonitrile (c = 1.0 μM) and the solid; (b) emission spectra of coated LED and blue LED; (c,h) optical and (d,i) fluorescence photographs of the solid powders of **S1** and **S2**; photographs of (e,j) uncoated LED bulb and coated LED bulb (f,g) before and (k,l) after illumination.

diameter of the **S1** aggregates reached 190 nm from the TEM images after adding 80% H_2O (Figure 3p). These results also were consistent with the AIE phenomenon of **S1**. Moreover, in order to obtain evidence for the aggregation behaviors, the dynamic light scattering (DLS) experiments were performed in a mixed DMF/H_2O solvent. The results are depicted in Figure 3j, in which the average hydrodynamic diameter of **S1** in DMF without H_2O is determined to be 4.85 nm, indicating no aggregation. The diameter of the aggregates changed from 18.2 to 225 nm, with the proportion of water increasing from 20 to 80%, demonstrating the formation of larger nanosphere structures in the DMF/H_2O system. **S2** shows a similar phenomenon to **S1** (Figure 3s−w). Interestingly, when the H_2O fraction was 80%, the size of **S2** aggregates had increased to 110 nm, which was slightly smaller than that of the **S1** aggregate at this point. The DLS results are also generally consistent with the TEM images (Figure 3q).

White Light Properties of S1 and S2 in Solution

Due to both the **S1** and **S2** emitting at 550 nm, which corresponds to a yellow emission region at high concentration (1.0×10^{-5} M), emission tuning experiments were performed by the blend of 9,10-dimethylanthracene (DMA) with a blue emission region.[83,84] Upon the addition of DMA with multiple emission peaks between 400 and 500 nm to a DMF solution of cages, the emission color was shifted from yellow to blue gradually (Figure 4a). At the amount of the guest molecule to 4.0 equiv, the two emission bands are perfectly balanced in proportion and a wide wavelength range covering 400−700 nm appears, resulting in white-light emission with a CIE coordinate at (0.32, 0.34)[85] (Figure 4b,c), the 6.0 and 8.0 equiv mixtures also have the same white emission. Similarly, the solution luminescence of **S2** gradually changed from yellow to white with the addition of DMA, and the full range of fluorescence emission appeared at the addition of 6.0 equiv DMA with a CIE coordinate at (0.31, 0.33) (Figure 4d−f). As can be seen, by the NMR spectra (Figure S35), there is no encapsulation relationship between the DMA and the metal-locages, instead, under intermolecular forces that make it distributed outside the supramolecular cage, it is considered that the WLE is achieved by doping. The excitation wavelengths of both the supramolecular structures **S1**, **S2**, and the DMA were at 330 nm, but one showed yellow light and the other had blue light, so the WLE was successfully achieved by superposition (Figure S42).

Solid-State Light-Emitting and White-Light Devices of S1 and S2

To determine the solid state tunable emission, we measured the emission of the cages in the solid state (Figure 5b). The fluorescence quantum yields of **S1** and **S2** in dilute solution are 0.56 and 2.3%, and the quantum yields of assembled supramolecular structure solids reached 23.4 and 12.3% (Figures 5a, S44 and S45),[74] which suggested that the solid emission of **S1** and **S2** can be enhanced by aggregation and coordination synergistically. The emission colors of supra-molecules **S1** and **S2** are all in the yellow region (Figure 5c,d,h and i), which complements the blue color, and they exhibited high quantum yield and good solution processability, which would enable applications in solid-state lighting. Therefore, the solids **S1** and **S2** were applied to create a white light-emitting diode by coating a blue light-emitting diode (LED) (Figure

https://doi.org/10.1021/jacsau.2c00568
JACS Au 2022, 2, 2809−2820

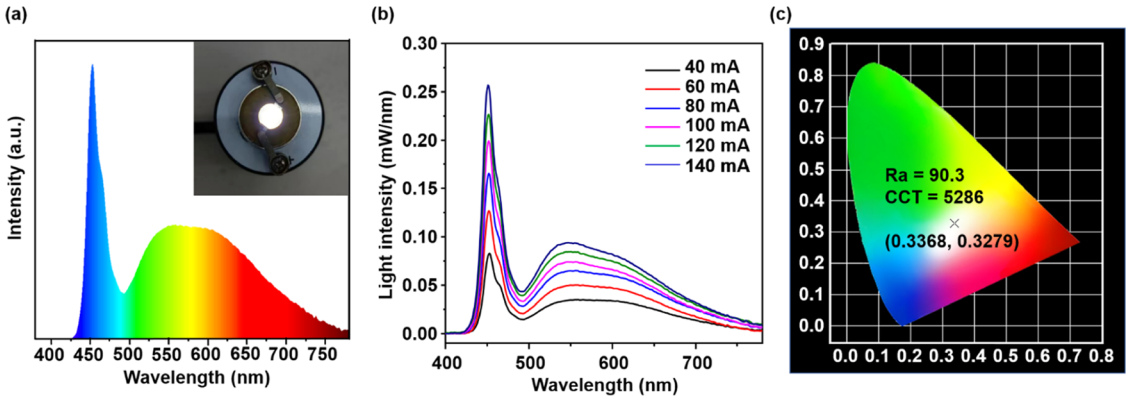

Figure 6. (a) Electroluminescence spectrum of the fabricated WLED prototype under a current of 40 mA. The inserted photograph shows the fabricated WLED prototype with a λ_{em} = 460 nm chip turned on under the drive current of 40 mA; (b) electroluminescence spectra of the natural WLED under different currents; (c) CIE coordinate diagram of the emission color at a current of 40 mA.

5e,j) bulb with the solution of **S1** and **S2**.[70,80,86] The blue LED bulb is simply dipped into an **S1** or **S2** solution of DMF and dried several times, and then a thin, uniform yellow film was formed on the surface of the bulb (Figure 5f,g). When a bias voltage of 3 V was applied, a visual white light was generated (Figure 5k,l), with a CIE coordinate at (0.34, 0.29) of **S1** (Figure S46). Compared with **S2**, **S1** has a higher fluorescence quantum yield and better WLE after coating the blue bulbs.

Given the fact that standard white light is defined as a point at 5500 K (0.33, 0.33),[87] even though the supramolecular solution was applied to the bulb to achieve white light, it did not achieve the desired color temperature and high color rendering index. Therefore, aiming to achieve more perfect white light performance, the well-executed **S1** sample was chosen to integrate with a 460 nm LED chip for fabricating a white light LED device based on a supramolecular cage, and performance tests were carried out. Also, the CIE color coordinates were applied to evaluate the quality of the constructed supramolecular cage-based white light-emitting diodes (WLEDs). The WLED prototypes consist of commercial near-UV-emitting LED (λ_{em} = 460 nm) chips (1 W, San'an Optoelectronics Co., Ltd) covered with a (Sr, Ba)$_2$SiO$_4$:Eu (1)/**S1** (4) film using organic silica gel.[88] The performance of the WLED device is shown in Figure 6c and Table S1. As shown in Figure 6b, the emission intensity of the device increased with the increase of the current from 40 to 140 mA at an interval of 20 mA. Especially, under a current of 40 mA (Figure 6a), the prototypes showed high-quality white light emission with a CIE coordinate of (0.34, 0.33), a high color rendering index (CRI, *Ra*) of 90.3, and a CCT of 5286 K (Figure 6c), which is very close to the ideal CIE for standard white emission (0.33, 0.33). The abovementioned values of the WLED prototypes under various currents were also measured (Table S1), and there was a steady variation of the chromaticity coordinates, which implies the stable light conversion and high color output quality of the natural WLED. The successful construction of this WLED prototype provides a theoretical basis for the application of tunable light-emitting supramolecular materials and broadens the range of applications of supramolecular materials.

CONCLUSIONS

In summary, two heterotopic terpyridine ligands with different arm lengths were designed and synthesized, and they were assembled with metal ions to obtain cuboctahedra metallocages **S1** and **S2**, which possessed tunable luminescence properties. Importantly, the optical properties of the two metallocages have been carefully investigated. Since both the coordination and aggregation states restrict intramolecular motion, solutions of these cages show remarkable AIE features, in which aggregation processes have been characterized by TEM and DLS tests. Based on the pronounced yellow emission of **S1** and **S2**, introducing blue emissive DMA in their solution can afford pure WLE. Due to the high fluorescence quantum yield and good solution processability of **S1** and **S2** in the solid state, they were used as coatings for blue LED bulbs to prepare white LED devices. To be noticed, stable light-conversion and high color output quality WLED prototypes were constructed successfully, which showed a high-quality white light, emission with a CIE coordinate of (0.3368, 0.3279). The successful preparation of metallocage with good emissive luminescence both in solution and solid states facilitates the application of supramolecular structures as practical emitter devices.

EXPERIMENTAL METHODS

Materials

Chemicals were purchased from Bidepharm, Sigma-Aldrich, Energy Chemical, and Alfa Aesar and used without further purification. Thin-layer chromatography (TLC) was conducted on flexible sheets (Baker-flex) precoated with Al_2O_3 (IB-F) or SiO_2 (IB2-F) and visualized by UV light. Column chromatography was conducted using neutral Al_2O_3 (200−300 mesh) SiO_2 (200−300 mesh). Different NMR solvents were purchased from Energy Chemical, J&K scientific, and Sigma-Aldrich.

General Instrumentation

^{1}H, ^{13}C, ^{19}F, ^{1}H−^{1}H COSY, ^{1}H−^{1}H NOESY NMR, and DOSY NMR spectra were recorded on a Bruker NMR. ESI-MS and TWIM-MS were recorded with a Waters Synapt G2-Si tandem mass spectrometer, using solutions of 0.01 mg of sample in 1 mL of $CHCl_3$/MeOH (1:3, v/v) for ligands or 0.5 mg of sample in 1 mL of DMF/MeOH (3:1, v/v) for complexes. TEM tests were performed on the JEOL JEM-2100F equipment. AFM imaging was performed on a Bruker Dimension Icon AFM system with ScanAsyst, and the data was processed by NanoScope Analysis version 2.0 (Bruker Software, Inc.). DLS was carried out on a Nano-ZS90 instrument at room temperature. Ultraviolet−visible spectroscopy (UV−vis) was recorded on Thermo Fisher Scientific Evolution 201 spectrophotometer. Fluorescence properties were measured using the Edinburgh-FS5 fluorescence spectrometer. Electronic absorption spectra in the visible region were recorded with a Shimadzu UV-3159 UV−vis−NIR

https://doi.org/10.1021/jacsau.2c00568
JACS Au 2022, 2, 2809−2820

spectrophotometer. The obtained NUV-WLEDs were tested by the Hongpu HP-9000 LED tester.

Synthesis of Ligand L1

Compound **1** (935 mg, 1.8 mmol), 4-tripyridine-phenylboric acid (3.81 g, 10.8 mmol), sodium carbonate (2.29 g, 21.6 mmol), and tetrakis(triphenylphosphine)palladium (416 mg, 0.36 mmol) were added to a 500 mL three-neck flask, and the entire reaction system was vacuumized and replaced with nitrogen three times to ensure that the entire reaction system was in a nitrogen atmosphere. Under these conditions, 120 mL of toluene, 24 mL of *tert*-butanol, and 48 mL of water were injected into the flask with a needle, followed by an ultrasound to ensure that the reactants were evenly dispersed, and the reaction was stirred at 80 °C for 4 days. At the end of the reaction, it was cooled to room temperature and extracted with dichloromethane and saturated salt water to collect the organic phase. The organic phase was dried with anhydrous Na_2SO_4, and the solvent was removed by vacuum distillation. The crude product had poor solubility, so it was purified by dry column chromatography (Al_2O_3), and DCM/MeOH (100:0.5, v/v) was used as the eluent to obtain 2 g of white solid (77% yield). ^{1}H NMR (400 MHz, $CDCl_3$, 300 K, ppm): δ 8.77 (s, 8H, tpy-$H^{3',5'}$), 8.68−8.64 (m, 16H, tpy-$H^{6,6''}$and tpy-$H^{3,3''}$), 7.96 (d, J = 8 Hz, 8H, Ph-H^a), 7.85 (t, J = 12 Hz, 8H, tpy-$H^{4,4''}$), 7.66 (d, J = 8 Hz, 8H, Ph-H^b), 7.31 (t, J = 12 Hz, 8H, tpy-$H^{5,5''}$), 7.15 (dd, J = 8, 4 Hz, 4H, Ph-H^c), 6.83 (dd, J = 8, 4 Hz, 4H, Ph-H^d); ^{13}C NMR (101 MHz, $CDCl_3$, 298 K): δ 156.27 (s), 155.86 (s), 149.92 (s), 149.11 (s), 143.03 (s), 138.67 (s), 137.44 (s), 136.88 (d, J = 14.2 Hz), 136.13 (s), 130.42 (s), 128.15 (s), 127.55 (s), 125.81 (s), 123.73 (s), 121.32 (s), 118.95 (s), 77.35 (s), 77.03 (s), 76.71 (s). ESI-TOF (m/z): Calcd. for $[C_{100}H_{64}N_{12}+H]^+$: 1434.54. Found: 1434.54.

Synthesis of Ligand L2

Compound **1** (100 mg, 0.192 mmol), compound **4** (590 mg, 1.154 mmol), Pd $(PPh_3)_4$ (44 mg, 0.2 mmol), and sodium carbonate (244 mg, 2.304 mmol) were added into a 250 mL three-necked flask. 50 mL of toluene, 30 mL of H_2O, and 20 mL of *tert*-butyl alcohol were added under N_2. The mixture was stirred at 85 °C for 4 days. After cooling to room temperature, the mixture was extracted with DCM. The combined organic layer was washed with brine, dried over anhydrous Na_2SO_4, and then concentrated in vacuo; the residue was purified by dry column chromatography (Al_2O_3), eluting with DCM/MeOH (100:1, v/v) to give the product as 150 mg of white solid (yield 44.9%). ^{1}H NMR (400 MHz, $CDCl_3$, 300 K, ppm): δ 8.80 (s, 8H, tpy-$H^{3',5'}$), 8.73 (d, J = 4.0 Hz, 8H, tpy-$H^{6,6''}$), 8.68 (d, J = 8 Hz, 8H, tpy-$H^{3,3''}$), 8.01 (d, J = 8 Hz, 8H, Ph-H^a), 7.88 (t, J = 12 Hz, 8H, tpy-$H^{4,4''}$), 7.80 (d, J = 8 Hz, 8H, Ph-H^b), 7.70 (d, J = 8 Hz, 8H, Ph-H^c), 7.62 (d, J = 8 Hz, 8H, Ph-H^d), 7.35 (t, J = 12 Hz, 8H, tpy-$H^{5,5''}$), 7.20 (dd, J = 8, 4 Hz, 4H, Ph-H^e), 6.86 (dd, J = 8, 4 Hz, 4H, Ph-H^f). ^{13}C NMR (101 MHz, $CDCl_3$, 298 K): δ 156.27 (s), 155.95 (s), 149.77 (s), 149.15 (s), 141.81 (s), 141.25 (s), 138.66 (s), 137.72 (s), 137.24 (s), 136.87 (s), 130.36 (s), 128.18 (s), 127.72 (s), 127.47 (s), 127.07 (s), 125.58 (s), 123.81 (s), 121.38 (s), 118.71 (s), 77.28 (d, J = 12 Hz), 77.02 (s), 76.70 (s). ESI-TOF (m/z): Calcd. for $[C_{124}H_{80}N_{12}+H]^+$: 1739.09. Found: 1739.09. (The experimental synthesis of compounds **1** and **4** can be found in the Supporting Information).

Synthesis of Complex S1 ($Zn_{24}L1_{12}$)

To a solution of ligand **L1** (5.0 mg, 3.48 μmol) in $CHCl_3$ (5 mL), a solution of $Zn(NTf_2)_2$ (4.36 mg, 6.96 μmol) in MeOH (10 mL) was added. The mixture was stirred at 55 °C for 6 h and then cooled to room temperature; then, 10-fold excess $LiNTf_2$ was added for the anion exchange, and a precipitate was formed, washed with water, and dried in a vacuum to give the product as a yellow solid (9.0 mg, 96.3%). ^{1}H NMR (400 MHz, CD_3CN, 300 K, ppm): δ 8.95 (s, 96H, tpy-$H^{3',5'}$), 8.70 (d, J = 8 Hz, 96H, tpy-$H^{3,3''}$), 8.23 (d, J = 8 Hz, 96H, Ph-H^a), 8.06−8.02 (m, 192H, tpy-$H^{4,4''}$ and Ph-H^b), 7.78 (br, 96H, tpy-$H^{6,6''}$), 7.49 (br, 48H, Ph-H^c), 7.32 (br, 96H, tpy-$H^{5,5''}$), 7.08 (br, 48H, Ph-H^d). ^{13}C NMR (126 MHz, CD_3CN, 298 K): δ 156.94 (s), δ 153.50 (s), δ 153.41 (s), 152.38 (s), 150.60 (s), 148.68 (s), 146.21 (s), 146.10 (s), 143.60 (s), 142.06 (s), 138.24 (s), 136.25 (s), 134.55 (s), 131.84 (s), 129.42 (s), 127.23 (s), 127.17 (s), 124.16 (s), 122.70 (s), 121.96 (s), 119.40 (s), 116.85 (s). ^{19}F NMR (376 MHz, CD_3CN, 298 K): δ −80.05 (s). ESI-TOF (m/z): 3299.83 $[M-9NTf_2^-]^{9+}$ (calcd m/z: 3299.83), 2941.86 $[M-10NTf_2^-]^{10+}$ (calcd m/z: 2941.86), 2649.05 $[M-11NTf_2^-]^{11+}$ (calcd m/z: 2649.05), 2404.90 $[M-12NTf_2^-]^{12+}$ (calcd m/z: 2404.90), 2198.61 $[M-13NTf_2^-]^{13+}$ (calcd m/z: 2198.61), 2021.54 $[M-14NTf_2^-]^{14+}$ (calcd m/z: 2021.54), 1868.16 $[M-15NTf_2^-]^{15+}$ (calcd m/z: 1868.16), 1733.83 $[M-16NTf_2^-]^{16+}$ (calcd m/z: 1733.83), 1615.40 $[M-17NTf_2^-]^{17+}$ (calcd m/z: 1615.40), 1510.09 $[M-18NTf_2^-]^{18+}$ (calcd m/z: 1510.09), 1415.83 $[M-19NTf_2^-]^{19+}$ (calcd m/z: 1415.83), 1331.09 $[M-20NTf_2^-]^{20+}$ (calcd m/z: 1331.09), 1254.29 $[M-21NTf_2^-]^{21+}$ (calcd m/z: 1254.29).

Synthesis of Complex S2 ($Zn_{24}L2_{12}$)

To a solution of ligand **L2** (5.0 mg, 2.87 μmol) in $CHCl_3$ (5 mL), a solution of $Zn(NTf_2)_2$ (3.599 mg, 5.74 μmol) in MeOH (10 mL) was added. The mixture was stirred at 55 °C for 6 h and then cooled to room temperature. Then, 10-fold excess $LiNTf_2$ was added for the anion exchange, and a precipitate was formed, washed with water, and dried in a vacuum to give the product as a solid (8.17 mg, 95.0%). ^{1}H NMR (400 MHz, CD_3CN, 300 K, ppm): δ 9.03 (s, 96H, tpy-$H^{3',5'}$), 8.74 (d, J = 8 Hz, 96H, tpy-$H^{3,3''}$), 8.31 (d, J = 8 Hz, 96H, Ph-H^a), 8.15 (t, J = 12 Hz, 96H, tpy-$H^{4,4''}$), 8.08 (d, J = 8 Hz, 96H, Ph-H^b), 7.93 (d, J = 8 Hz, 96H, Ph-H^c), 7.85−7.84 (m, 192H, tpy-$H^{6,6''}$ and Ph-H^d), 7.40−7.37 (m, 144H, tpy-$H^{5.5''}$ and Ph-H^e), 6.97 (s, 48H, Ph-H^f). ^{13}C NMR (126 MHz, CD_3CN, 298 K): δ 156.75 (s), 150.72 (s), 148.79 (s), 143.86 (s), 142.12 (s), 138.85 (s), 136.07 (s), 131.30 (s), 129.60 (s), 128.51 (s), 126.72 (s), 124.14 (s), 122.29 (s), 122.04 (s), 119.49 (s). ^{19}F NMR (376 MHz, CD_3CN, 298 K): δ −80.11 (s). ESI-TOF (m/z): 2981.81 $[M-11NTf_2^-]^{11+}$ (calcd m/z: 2981.81), 2709.77 $[M-12NTf_2^-]^{12+}$ (calcd m/z: 2709.77), 2479.87 $[M-13NTf_2^-]^{13+}$ (calcd m/z: 2479.87), 2282.85 $[M-14NTf_2^-]^{14+}$ (calcd m/z: 2282.85), 2111.98 $[M-15NTf_2^-]^{15+}$ (calcd m/z: 2111.98), 1962.41 $[M-16NTf_2^-]^{16+}$ (calcd m/z: 1962.41), 1830.51 $[M-17NTf_2^-]^{17+}$ (calcd m/z: 1830.51), 1713.25 $[M-18NTf_2^-]^{18+}$ (calcd m/z: 1713.25), 1608.28 $[M-19NTf_2^-]^{19+}$ (calcd m/z: 1608.28), 1512.96 $[M-20NTf_2^-]^{20+}$ (calcd m/z: 1512.96), 1428.44 $[M-21NTf_2^-]^{21+}$ (calcd m/z: 1428.44), 1350.73 $[M-22NTf_2^-]^{22+}$ (calcd m/z: 1350.73), 1250.89 $[M-23NTf_2^-]^{23+}$ (calcd m/z: 1250.89), 1214.99 $[M-24NTf_2^-]^{24+}$ (calcd m/z: 1214.99).

■ ASSOCIATED CONTENT

Supporting Information

The Supporting Information is available free of charge at https://pubs.acs.org/doi/10.1021/jacsau.2c00568.

Characterization methods, experimental details, theoretical calculation details, and characterization of compounds (PDF)

■ AUTHOR INFORMATION

Corresponding Authors

Pei-Yang Su − *Institute of Environmental Research at Greater Bay Area, Key Laboratory for Water Quality and Conservation of the Pearl River Delta, Ministry of Education, Guangzhou University, Guangzhou 510006, China*; Email: supy@gzhu.edu.cn

Ting-Zheng Xie − *Institute of Environmental Research at Greater Bay Area, Key Laboratory for Water Quality and Conservation of the Pearl River Delta, Ministry of Education, Guangzhou University, Guangzhou 510006, China*; orcid.org/0000-0001-6717-7642; Email: xietingzheng@gzhu.edu.cn

Pingshan Wang − *Institute of Environmental Research at Greater Bay Area, Key Laboratory for Water Quality and*

Conservation of the Pearl River Delta, Ministry of Education, Guangzhou University, Guangzhou 510006, China; Hunan Key Laboratory of Micro & Nano Materials Interface Science; College of Chemistry and Chemical Engineering, Central South University, Changsha 410083, China; orcid.org/0000-0002-1988-7604; Email: chemwps@csu.edu.cn

Authors

Zhe Zhang − *Institute of Environmental Research at Greater Bay Area, Key Laboratory for Water Quality and Conservation of the Pearl River Delta, Ministry of Education, Guangzhou University, Guangzhou 510006, China*

Yan Huang − *Institute of Environmental Research at Greater Bay Area, Key Laboratory for Water Quality and Conservation of the Pearl River Delta, Ministry of Education, Guangzhou University, Guangzhou 510006, China*

Qixia Bai − *Institute of Environmental Research at Greater Bay Area, Key Laboratory for Water Quality and Conservation of the Pearl River Delta, Ministry of Education, Guangzhou University, Guangzhou 510006, China*

Tun Wu − *Institute of Environmental Research at Greater Bay Area, Key Laboratory for Water Quality and Conservation of the Pearl River Delta, Ministry of Education, Guangzhou University, Guangzhou 510006, China*

Zhiyuan Jiang − *Hunan Key Laboratory of Micro & Nano Materials Interface Science; College of Chemistry and Chemical Engineering, Central South University, Changsha 410083, China*

Haoyue Su − *State Key Laboratory of Supramolecular Structure and Materials, College of Chemistry, Jilin University, Changchun, Jilin 130012, China*

Yingxin Zong − *Institute of Environmental Research at Greater Bay Area, Key Laboratory for Water Quality and Conservation of the Pearl River Delta, Ministry of Education, Guangzhou University, Guangzhou 510006, China*

Ming Wang − *State Key Laboratory of Supramolecular Structure and Materials, College of Chemistry, Jilin University, Changchun, Jilin 130012, China;* orcid.org/0000-0002-5332-0804

Complete contact information is available at: https://pubs.acs.org/10.1021/jacsau.2c00568

Author Contributions

[⊥]Z.Z., Y.H., and Q.B. contributed equally to this work. P.W. and Z.Z. conceived the project. Y.H. performed the synthesis and characterization experiments. Z.Z. and Q.B. performed the MS measurements. T.W. and Z.J. performed the NMR studies. Y.H. analyzed and organized the data. Y.Z. did the TEM tests. M.W. and H.S. did the AFM tests. P.S. performed experiments on white light devices. Q.B. and Z.Z. drafted the manuscript. T.-Z. X and P.W. oversaw the project. All authors discussed the results and commented on the paper.

Notes

The authors declare no competing financial interest.

■ ACKNOWLEDGMENTS

This research was supported by the National Natural Science Foundation of China (22101061 to Z.Z., 21971257 to P.W., 21971048 to T.-Z.X., and 21806027 to P.S.), the Science and Technology Research Project of Guangzhou (202002030257 to Z.Z.), the Guangdong Provincial Pearl River Talents Program (2019QN01C243 to T.-Z.X.), and the Natural Science Foundation of Guangdong Province (2018A030313479 to P.S.). We thank the staff from the BL17B1 beamline of the National Facility for Protein Science at the Shanghai Synchrotron Radiation Facility for their assistance during data collection.

■ REFERENCES

(1) Borisov, S. M.; Krause, C.; Arain, S.; Wolfbeis, O. S. Composite Material for Simultaneous and Contactless Luminescent Sensing and Imaging of Oxygen and Carbon Dioxide. *Adv. Mater.* **2006**, *18*, 1511−1516.

(2) Hong, Y.; Meng, L.; Chen, S.; Leung, C. W. T.; Da, L.-T.; Faisal, M.; Silva, D.-A.; Liu, J.; Lam, J. W. Y.; Huang, X.; Tang, B. Z. Monitoring and Inhibition of Insulin Fibrillation by a Small Organic Fluorogen with Aggregation-Induced Emission Characteristics. *J. Am. Chem. Soc.* **2012**, *134*, 1680−1689.

(3) Mako, T. L.; Racicot, J. M.; Levine, M. Supramolecular Luminescent Sensors. *Chem. Rev.* **2019**, *119*, 322−477.

(4) Sinn, S.; Biedermann, F.; Vishe, M.; Aliprandi, A.; Besnard, C.; Lacour, J.; De Cola, L. A Ratiometric Luminescent Switch Based on Platinum Complexes Tethered to a Crown-Ether Scaffold. *ChemPhysChem* **2016**, *17*, 1829−1834.

(5) Wu, W.-C.; Chen, C.-Y.; Tian, Y.; Jang, S.-H.; Hong, Y.; Liu, Y.; Hu, R.; Tang, B. Z.; Lee, Y.-T.; Chen, C.-T.; Chen, W.-C.; Jen, A. K. Y. Enhancement of Aggregation-Induced Emission in Dye-Encapsulating Polymeric Micelles for Bioimaging. *Adv. Funct. Mater.* **2010**, *20*, 1413−1423.

(6) Yang, Y.; Zhao, Q.; Feng, W.; Li, F. Luminescent Chemodosimeters for Bioimaging. *Chem. Rev.* **2013**, *113*, 192−270.

(7) Zhou, J.; Zhang, Y.; Yu, G.; Crawley, M. R.; Fulong, C. R. P.; Friedman, A. E.; Sengupta, S.; Sun, J.; Li, Q.; Huang, F.; Cook, T. R. Highly Emissive Self-Assembled BODIPY-Platinum Supramolecular Triangles. *J. Am. Chem. Soc.* **2018**, *140*, 7730−7736.

(8) Qi, Q.; Li, C.; Liu, X.; Jiang, S.; Xu, Z.; Lee, R.; Zhu, M.; Xu, B.; Tian, W. Solid-State Photoinduced Luminescence Switch for Advanced Anticounterfeiting and Super-Resolution Imaging Applications. *J. Am. Chem. Soc.* **2017**, *139*, 16036−16039.

(9) Tian, W.; Zhang, J.; Yu, J.; Wu, J.; Zhang, J.; He, J.; Wang, F. Phototunable Full-Color Emission of Cellulose-Based Dynamic Fluorescent Materials. *Adv. Funct. Mater.* **2018**, *28*, 1703548−1703557.

(10) Gao, M.; Yu, F.; Lv, C.; Choo, J.; Chen, L. Fluorescent chemical probes for accurate tumor diagnosis and targeting therapy. *Chem. Soc. Rev.* **2017**, *46*, 2237−2271.

(11) Hu, Y.-X.; Hao, X.; Xu, L.; Xie, X.; Xiong, B.; Hu, Z.; Sun, H.; Yin, G.-Q.; Li, X.; Peng, H.; Yang, H.-B. Construction of Supramolecular Liquid-Crystalline Metallacycles for Holographic Storage of Colored Images. *J. Am. Chem. Soc.* **2020**, *142*, 6285−6294.

(12) Yan, X.; Wei, P.; Liu, Y.; Wang, M.; Chen, C.; Zhao, J.; Li, G.; Saha, M. L.; Zhou, Z.; An, Z.; Li, X.; Stang, P. J. Endo- and Exo-Functionalized Tetraphenylethylene $M_{12}L_{24}$ Nanospheres: Fluorescence Emission inside a Confined Space. *J. Am. Chem. Soc.* **2019**, *141*, 9673−9679.

(13) Hong, Y.; Lam, J. W. Y.; Tang, B. Z. Aggregation-induced emission. *Chem. Soc. Rev.* **2011**, *40*, 5361−5388.

(14) Ding, D.; Li, K.; Liu, B.; Tang, B. Z. Bioprobes Based on AIE Fluorogens. *Acc. Chem. Res.* **2013**, *46*, 2441−2453.

(15) Chen, Y.; Pang, X.-H.; Dong, C.-M. Dual Stimuli-Responsive Supramolecular Polypeptide-Based Hydrogel and Reverse Micellar Hydrogel Mediated by Host-Guest Chemistry. *Adv. Funct. Mater.* **2010**, *20*, 579−586.

(16) Mei, J.; Leung, N. L. C.; Kwok, R. T. K.; Lam, J. W. Y.; Tang, B. Z. Aggregation-Induced Emission: Together We Shine, United We Soar. *Chem. Rev.* **2015**, *115*, 11718−11940.

(17) Luo, J.; Xie, Z.; Lam, J. W. Y.; Cheng, L.; Tang, H.; Chen, C.; Qiu, H. S.; Kwok, X.; Zhan, Y.; Liu, D.; Zhu, B. Z. Aggregation-

induced emission of 1-methyl-1,2,3,4,5-pentaphenylsilole. *Chem. Commun.* **2001**, 1740−1741.
(18) Wang, Y.; Chen, S.; Qiu, L.; Wang, K.; Wang, H.; Simon, G. P.; Li, D. Graphene-Directed Supramolecular Assembly of Multifunctional Polymer Hydrogel Membranes. *Adv. Funct. Mater.* **2015**, *25*, 126−133.
(19) Jin, G.; Liu, J.-Z.; Zou, J.-H.; Huang, X.-L.; He, M.-J.; Peng, L.; Chen, L.-L.; Zhu, X.-H.; Peng, J.; Cao, Y. Appending triphenyltriazine to 1,10-phenanthroline: a robust electron-transport material for stable organic light-emitting diodes. *Sci. Bull.* **2018**, *63*, 446−451.
(20) Wong, M. Y.; Zysman-Colman, E. Purely Organic Thermally Activated Delayed Fluorescence Materials for Organic Light-Emitting Diodes. *Adv. Mater.* **2017**, *29*, 1605444−1605497.
(21) Zhang, Y.-L.; Ran, Q.; Wang, Q.; Fan, J.; Liao, L.-S. High-efficiency exciplex-based white organic light-emitting diodes with a new tripodal material as a co-host. *J. Mater. Chem. C* **2019**, *7*, 7267−7272.
(22) Li, M.; Liu, Y.; Duan, R.; Wei, X.; Yi, Y.; Wang, Y.; Chen, C.-F. Aromatic-Imide-Based Thermally Activated Delayed Fluorescence Materials for Highly Efficient Organic Light-Emitting Diodes. *Angew. Chem., Int. Ed.* **2017**, *56*, 8818−8822.
(23) Zhang, Z.; Li, Y.; Song, B.; Zhang, Y.; Jiang, X.; Wang, M.; Tumbleson, R.; Liu, C.; Wang, P.; Hao, X.-Q.; Rojas, T.; Ngo, A. T.; Sessler, J. L.; Newkome, G. R.; Hla, S. W.; Li, X. Intra- and intermolecular self-assembly of a 20-nm-wide supramolecular hexagonal grid. *Nat. Chem.* **2020**, *12*, 468−474.
(24) Romuald, C.; Coutrot, F. Combining Coordination Chemistry and Catalysis To Tie a Knot by an Active-Metal Template Strategy. *Angew. Chem., Int. Ed.* **2012**, *51*, 2544−2545.
(25) Heo, J.; Jeon, Y.-M.; Mirkin, C. A. Reversible Interconversion of Homochiral Triangular Macrocycles and Helical Coordination Polymers. *J. Am. Chem. Soc.* **2007**, *129*, 7712−7713.
(26) Danon, J. J.; Krüger, A.; Leigh, D. A.; Lemonnier, J.-F.; Stephens, A. J.; Vitorica-Yrezabal, I. J.; Woltering, S. L. Braiding a molecular knot with eight crossings. *Science* **2017**, *355*, 159−162.
(27) Zhang, L.; Stephens, A. J.; Nussbaumer, A. L.; Lemonnier, J.-F.; Jurček, P.; Vitorica-Yrezabal, I. J.; Leigh, D. A. Stereoselective synthesis of a composite knot with nine crossings. *Nat. Chem.* **2018**, *10*, 1083−1088.
(28) Chichak, K. S.; Cantrill, S. J.; Pease, A. R.; Chiu, S.-H.; Cave, G. W. V.; Atwood, J. L.; Stoddart, J. F. Molecular Borromean Rings. *Science* **2004**, *304*, 1308−1312.
(29) Newkome, G. R.; Wang, P.; Moorefield, C. N.; Cho, T. J.; Mohapatra, P. P.; Li, S.; Hwang, S.-H.; Lukoyanova, O.; Echegoyen, L.; Palagallo, J. A.; Iancu, V.; Hla, S.-W. Nanoassembly of a Fractal Polymer: A Molecular "Sierpinski Hexagonal Gasket". *Science* **2006**, *312*, 1782−1785.
(30) Sun, Y.; Chen, C.; Liu, J.; Stang, P. J. Recent developments in the construction and applications of platinum-based metallacycles and metallacages via coordination. *Chem. Soc. Rev.* **2020**, *49*, 3889−3919.
(31) Chakraborty, S.; Newkome, G. R. Terpyridine-based metallosupramolecular constructs: tailored monomers to precise 2D-motifs and 3D-metallocages. *Chem. Soc. Rev.* **2018**, *47*, 3991−4016.
(32) Koo, J.; Kim, I.; Kim, Y.; Cho, D.; Hwang, I.-C.; Mukhopadhyay, R. D.; Song, H.; Ko, Y. H.; Dhamija, A.; Lee, H.; Hwang, W.; Kim, S.; Baik, M.-H.; Kim, K. Gigantic Porphyrinic Cages. *Chem* **2020**, *6*, 3374−3384.
(33) Wang, H.; Wang, K.; Xu, Y.; Wang, W.; Chen, S.; Hart, M.; Wojtas, L.; Zhou, L.-P.; Gan, L.; Yan, X.; Li, Y.; Lee, J.; Ke, X.-S.; Wang, X.-Q.; Zhang, C.-W.; Zhou, S.; Zhai, T.; Yang, H.-B.; Wang, M.; He, J.; Sun, Q.-F.; Xu, B.; Jiao, Y.; Stang, P. J.; Sessler, J. L.; Li, X. Hierarchical Self-Assembly of Nanowires on the Surface by Metallo-Supramolecular Truncated Cuboctahedra. *J. Am. Chem. Soc.* **2021**, *143*, 5826−5835.
(34) Gu, Y.; Alt, E. A.; Wang, H.; Li, X.; Willard, A. P.; Johnson, J. A. Photoswitching topology in polymer networks with metal−organic cages as crosslinks. *Nature* **2018**, *560*, 65−69.
(35) Xie, T.-Z.; Guo, K.; Guo, Z.; Gao, W.-Y.; Wojtas, L.; Ning, G.-H.; Huang, M.; Lu, X.; Li, J.-Y.; Liao, S.-Y.; Chen, Y.-S.; Moorefield, C. N.; Saunders, M. J.; Cheng, S. Z. D.; Wesdemiotis, C.; Newkome, G. R. Precise Molecular Fission and Fusion: Quantitative Self-Assembly and Chemistry of a Metallo-Cuboctahedron. *Angew. Chem., Int. Ed.* **2015**, *54*, 9224−9229.
(36) Sun, Q.-F.; Iwasa, J.; Ogawa, D.; Ishido, Y.; Sato, S.; Ozeki, T.; Sei, Y.; Yamaguchi, K.; Fujita, M. Self-Assembled $M_{24}L_{48}$ Polyhedra and Their Sharp Structural Switch upon Subtle Ligand Variation. *Science* **2010**, *328*, 1144−1147.
(37) Sudik, A. C.; Millward, A. R.; Ockwig, N. W.; Côté, A. P.; Kim, J.; Yaghi, O. M. Design, Synthesis, Structure, and Gas (N_2, Ar, CO_2, CH_4, and H_2) Sorption Properties of Porous Metal-Organic Tetrahedral and Heterocuboidal Polyhedra. *J. Am. Chem. Soc.* **2005**, *127*, 7110−7118.
(38) Pilgrim, B. S.; Roberts, D. A.; Lohr, T. G.; Ronson, T. K.; Nitschke, J. R. Signal transduction in a covalent post-assembly modification cascade. *Nat. Chem.* **2017**, *9*, 1276−1281.
(39) Fujita, D.; Ueda, Y.; Sato, S.; Yokoyama, H.; Mizuno, N.; Kumasaka, T.; Fujita, M. Self-Assembly of $M_{30}L_{60}$ Icosidodecahedron. *Chem* **2016**, *1*, 91−101.
(40) Bhattacharyya, A.; De Sarkar, S.; Das, A. Supramolecular Engineering and Self-Assembly Strategies in Photoredox Catalysis. *ACS Catal.* **2021**, *11*, 710−733.
(41) Zhu, F.-F.; Chen, L.-J.; Chen, S.; Wu, G.-Y.; Jiang, W.-L.; Shen, J.-C.; Qin, Y.; Xu, L.; Yang, H.-B. Confinement Self-Assembly of Metal-Organic Cages within Mesoporous Carbon for One-Pot Sequential Reactions. *Chem* **2020**, *6*, 2395−2406.
(42) Ngai, C.; Sanchez-Marsetti, C. M.; Harman, W. H.; Hooley, R. J. Supramolecular Catalysis of the oxa-Pictet−Spengler Reaction with an Endohedrally Functionalized Self-Assembled Cage Complex. *Angew. Chem., Int. Ed.* **2020**, *59*, 23505−23509.
(43) Schulze, M.; Kunz, V.; Frischmann, P. D.; Würthner, F. A supramolecular ruthenium macrocycle with high catalytic activity for water oxidation that mechanistically mimics photosystem II. *Nat. Chem.* **2016**, *8*, 576−583.
(44) Wang, J.; He, C.; Wu, P.; Wang, J.; Duan, C. An Amide-Containing Metal−Organic Tetrahedron Responding to a Spin-Trapping Reaction in a Fluorescent Enhancement Manner for Biological Imaging of NO in Living Cells. *J. Am. Chem. Soc.* **2011**, *133*, 12402−12405.
(45) Li, K.; Zhang, L.-Y.; Yan, C.; Wei, S.-C.; Pan, M.; Zhang, L.; Su, C.-Y. Stepwise Assembly of Pd6(RuL3)8 Nanoscale Rhombododecahedral Metal−Organic Cages via Metalloligand Strategy for Guest Trapping and Protection. *J. Am. Chem. Soc.* **2014**, *136*, 4456−4459.
(46) Duan, H.; Li, Y.; Li, Q.; Wang, P.; Liu, X.; Cheng, L.; Yu, Y.; Cao, L. Host−Guest Recognition and Fluorescence of a Tetraphenylethene-Based Octacationic Cage. *Angew. Chem., Int. Ed.* **2020**, *59*, 10101−10110.
(47) Zhang, D.; Ronson, T. K.; Zou, Y.-Q.; Nitschke, J. R. Metal−organic cages for molecular separations. *Nat. Rev. Chem.* **2021**, *5*, 168−182.
(48) Grommet, A. B.; Nitschke, J. R. Directed Phase Transfer of an $FeII_4L_4$ Cage and Encapsulated Cargo. *J. Am. Chem. Soc.* **2017**, *139*, 2176−2179.
(49) Masar, M. S.; Gianneschi, N. C.; Oliveri, C. G.; Stern, C. L.; Nguyen, S. T.; Mirkin, C. A. Allosterically Regulated Supramolecular Catalysis of Acyl Transfer Reactions for Signal Amplification and Detection of Small Molecules. *J. Am. Chem. Soc.* **2007**, *129*, 10149−10158.
(50) Liu, Y.; Sengupta, A.; Raghavachari, K.; Flood, A. H. Anion Binding in Solution: Beyond the Electrostatic Regime. *Chem* **2017**, *3*, 411−427.
(51) Rizzuto, F. J.; von Krbek, L. K. S.; Nitschke, J. R. Strategies for binding multiple guests in metal−organic cages. *Nat. Rev. Chem.* **2019**, *3*, 204−222.
(52) Jung, M.; Kim, H.; Baek, K.; Kim, K. Synthetic Ion Channel Based on Metal−Organic Polyhedra. *Angew. Chem., Int. Ed.* **2008**, *47*, 5755−5757.
(53) Shustova, N. B.; McCarthy, B. D.; Dincă, M. Turn-On Fluorescence in Tetraphenylethylene-Based Metal−Organic Frame-

https://doi.org/10.1021/jacsau.2c00568
JACS Au 2022, 2, 2809−2820

works: An Alternative to Aggregation-Induced Emission. *J. Am. Chem. Soc.* **2011**, *133*, 20126−20129.
(54) Hu, X.; Liu, F.; Zhang, X.; Zhao, Z.; Liu, S. Expected and unexpected photoreactions of 9-(10-)substituted anthracene derivatives in cucurbit[n]uril hosts. *Chem. Sci.* **2020**, *11*, 4779−4785.
(55) Zhu, Z.-H.; Ni, Z.; Zou, H.-H.; Feng, G.; Tang, B. Z. Smart Metal−Organic Frameworks with Reversible Luminescence/Magnetic Switch Behavior for HCl Vapor Detection. *Adv. Funct. Mater.* **2021**, *31*, 2106925−2106934.
(56) Zhu, Z.-H.; Bi, C.; Zou, H.-H.; Feng, G.; Xu, S.; Tang, B. Z. Smart Tetraphenylethene-Based Luminescent Metal−Organic Frameworks with Amide-Assisted Thermofluorochromics and Piezofluorochromics. *Adv. Sci.* **2022**, *9*, 2200850−2200858.
(57) Zhu, L.; Zhu, B.; Luo, J.; Liu, B. Design and Property Modulation of Metal−Organic Frameworks with Aggregation-Induced Emission. *ACS Mater. Lett.* **2021**, *3*, 77−89.
(58) Zhang, M.; Feng, G.; Song, Z.; Zhou, Y.-P.; Chao, H.-Y.; Yuan, D.; Tan, T. T. Y.; Guo, Z.; Hu, Z.; Tang, B. Z.; Liu, B.; Zhao, D. Two-Dimensional Metal−Organic Framework with Wide Channels and Responsive Turn-On Fluorescence for the Chemical Sensing of Volatile Organic Compounds. *J. Am. Chem. Soc.* **2014**, *136*, 7241−7244.
(59) Zhou, Z.; Yan, X.; Saha, M. L.; Zhang, M.; Wang, M.; Li, X.; Stang, P. J. Immobilizing Tetraphenylethylene into Fused Metallacycles: Shape Effects on Fluorescence Emission. *J. Am. Chem. Soc.* **2016**, *138*, 13131−13134.
(60) Yin, G.-Q.; Wang, H.; Wang, X.-Q.; Song, B.; Chen, L.-J.; Wang, L.; Hao, X.-Q.; Yang, H.-B.; Li, X. Self-assembly of emissive supramolecular rosettes with increasing complexity using multitopic terpyridine ligands. *Nat. Commun.* **2018**, *9*, 567−577.
(61) Yan, X.; Wang, H.; Hauke, C. E.; Cook, T. R.; Wang, M.; Saha, M. L.; Zhou, Z.; Zhang, M.; Li, X.; Huang, F.; Stang, P. J. A Suite of Tetraphenylethylene-Based Discrete Organoplatinum(II) Metallacycles: Controllable Structure and Stoichiometry, Aggregation-Induced Emission, and Nitroaromatics Sensing. *J. Am. Chem. Soc.* **2015**, *137*, 15276−15286.
(62) Feng, H.-T.; Yuan, Y.-X.; Xiong, J.-B.; Zheng, Y.-S.; Tang, B. Z. Macrocycles and cages based on tetraphenylethylene with aggregation-induced emission effect. *Chem. Soc. Rev.* **2018**, *47*, 7452−7476.
(63) Zhang, M.; Saha, M. L.; Wang, M.; Zhou, Z.; Song, B.; Lu, C.; Yan, X.; Li, X.; Huang, F.; Yin, S.; Stang, P. J. Multicomponent Platinum(II) Cages with Tunable Emission and Amino Acid Sensing. *J. Am. Chem. Soc.* **2017**, *139*, 5067−5074.
(64) Yu, G.; Cook, T. R.; Li, Y.; Yan, X.; Wu, D.; Shao, L.; Shen, J.; Tang, G.; Huang, F.; Chen, X.; Stang, P. J. Tetraphenylethene-based highly emissive metallacage as a component of theranostic supramolecular nanoparticles. *Proc. Natl. Acad. Sci.* **2016**, *113*, 13720−13725.
(65) Wang, Q.; Zhang, Q.; Zhang, Q.-W.; Li, X.; Zhao, C.-X.; Xu, T.-Y.; Qu, D.-H.; Tian, H. Color-tunable single-fluorophore supramolecular system with assembly-encoded emission. *Nat. Commun.* **2020**, *11*, 158−167.
(66) Li, G.; Zhou, Z.; Yuan, C.; Guo, Z.; Liu, Y.; Zhao, D.; Liu, K.; Zhao, J.; Tan, H.; Yan, X. Trackable Supramolecular Fusion: Cage to Cage Transformation of Tetraphenylethylene-Based Metalloassemblies. *Angew. Chem., Int. Ed.* **2020**, *59*, 10013−10017.
(67) Guo, Z.; Li, G.; Wang, H.; Zhao, J.; Liu, Y.; Tan, H.; Li, X.; Stang, P. J.; Yan, X. Drum-like Metallacages with Size-Dependent Fluorescence: Exploring the Photophysics of Tetraphenylethylene under Locked Conformations. *J. Am. Chem. Soc.* **2021**, *143*, 9215−9221.
(68) Pan, M.; Liao, W.-M.; Yin, S.-Y.; Sun, S.-S.; Su, C.-Y. Single-Phase White-Light-Emitting and Photoluminescent Color-Tuning Coordination Assemblies. *Chem. Rev.* **2018**, *118*, 8889−8935.
(69) Ma, X.; Jia, L.; Yang, B.; Li, J.; Huang, W.; Wu, D.; Wong, W.-Y. A color-tunable single molecule white light emitter with high luminescence efficiency and ultra-long room temperature phosphorescence. *J. Mater. Chem. C* **2021**, *9*, 727−735.
(70) Li, Q.; Wu, Y.; Cao, J.; Liu, Y.; Wang, Z.; Zhu, H.; Zhang, H.; Huang, F. Pillararene-Induced Intramolecular Through-Space Charge Transfer and Single-Molecule White-Light Emission. *Angew. Chem., Int. Ed.* **2022**, *61*, No. e202202381.
(71) Hu, J.; Li, Q.; Wang, X.; Shao, S.; Wang, L.; Jing, X.; Wang, F. Developing Through-Space Charge Transfer Polymers as a General Approach to Realize Full-Color and White Emission with Thermally Activated Delayed Fluorescence. *Angew. Chem., Int. Ed.* **2019**, *58*, 8405−8409.
(72) Chen, Z.; Ho, C.-L.; Wang, L.; Wong, W.-Y. Single-Molecular White-Light Emitters and Their Potential WOLED Applications. *Adv. Mater.* **2020**, *32*, 1903269−1903313.
(73) Chen, M.; Zhao, Y.; Yan, L.; Yang, S.; Zhu, Y.; Murtaza, I.; He, G.; Meng, H.; Huang, W. A Unique Blend of 2-Fluorenyl-2-anthracene and 2-Anthryl-2-anthracence Showing White Emission and High Charge Mobility. *Angew. Chem., Int. Ed.* **2017**, *56*, 722−727.
(74) Mu, C.; Zhang, Z.; Hou, Y.; Liu, H.; Ma, L.; Li, X.; Ling, S.; He, G.; Zhang, M. Tetraphenylethylene-Based Multicomponent Emissive Metallacages as Solid-State Fluorescent Materials. *Angew. Chem., Int. Ed.* **2021**, *60*, 12293−12297.
(75) Neelakandan, P. P.; Jiménez, A.; Nitschke, J. R. Fluorophore incorporation allows nanomolar guest sensing and white-light emission in M_4L_6 cage complexes. *Chem. Sci.* **2014**, *5*, 908−915.
(76) Jia, S.; Xiao, X.; Li, Q.; Li, Y.; Duan, Z.; Li, Y.; Li, X.; Lin, Z.; Zhao, Y.; Huang, W. Tuning the Connectivity, Rigidity, and Functionality of Two-Dimensional Zr-Based Metal−Organic Frameworks. *Inorg. Chem.* **2019**, *58*, 12748−12755.
(77) Chan, Y.-T.; Li, X.; Yu, J.; Carri, G. A.; Moorefield, C. N.; Newkome, G. R.; Wesdemiotis, C. Design, Synthesis, and Traveling Wave Ion Mobility Mass Spectrometry Characterization of Iron(II)− and Ruthenium(II)−Terpyridine Metallomacrocycles. *J. Am. Chem. Soc.* **2011**, *133*, 11967−11976.
(78) Zhang, Z.; Zhao, Z.; Hou, Y.; Wang, H.; Li, X.; He, G.; Zhang, M. Aqueous Platinum(II)-Cage-Based Light-Harvesting System for Photocatalytic Cross-Coupling Hydrogen Evolution Reaction. *Angew. Chem., Int. Ed.* **2019**, *58*, 8862−8866.
(79) Yu, J.-G.; Sun, L.-Y.; Wang, C.; Li, Y.; Han, Y.-F. Coordination-Induced Emission from Tetraphenylethylene Units and Their Applications. *Chem.−Eur. J.* **2021**, *27*, 1556−1575.
(80) Yan, X.; Cook, T. R.; Wang, P.; Huang, F.; Stang, P. J. Highly emissive platinum(II) metallacages. *Nat. Chem.* **2015**, *7*, 342−348.
(81) Dong, J.; Pan, Y.; Wang, H.; Yang, K.; Liu, L.; Qiao, Z.; Yuan, Y. D.; Peh, S. B.; Zhang, J.; Shi, L.; Liang, H.; Han, Y.; Li, X.; Jiang, J.; Liu, B.; Zhao, D. Self-Assembly of Highly Stable Zirconium(IV) Coordination Cages with Aggregation Induced Emission Molecular Rotors for Live-Cell Imaging. *Angew. Chem., Int. Ed.* **2020**, *59*, 10151−10159.
(82) Wang, X.-y.; Del Guerzo, A.; Schmehl, R. H. Preferential solvation of an ILCT excited state in bis(terpyridine−phenylene−vinylene) Zn(ii) complexes. *Chem. Commun.* **2002**, 2344−2345.
(83) Hou, Y.; Zhang, Z.; Lu, S.; Yuan, J.; Zhu, Q.; Chen, W.-P.; Ling, S.; Li, X.; Zheng, Y.-Z.; Zhu, K.; Zhang, M. Highly Emissive Perylene Diimide-Based Metallacages and Their Host−Guest Chemistry for Information Encryption. *J. Am. Chem. Soc.* **2020**, *142*, 18763−18768.
(84) Zhang, M.; Yin, S.; Zhang, J.; Zhou, Z.; Saha, M. L.; Lu, C.; Stang, P. J. Metallacycle-cored supramolecular assemblies with tunable fluorescence including white-light emission. *Proc. Natl. Acad. Sci. U.S.A.* **2017**, *114*, 3044−3049.
(85) Smith, T. The C.I.E. colorimetric standards and their use. *Trans. Opt. Soc.* **1931**, *33*, 73−134.
(86) Skonieczny, K.; Yoo, J.; Larsen, J. M.; Espinoza, E. M.; Barbasiewicz, M.; Vullev, V. I.; Lee, C.-H.; Gryko, D. T. How To Reach Intense Luminescence for Compounds Capable of Excited-State Intramolecular Proton Transfer? *Chem. - Eur. J.* **2016**, *22*, 7485−7496.
(87) Xu, C.; Guan, H.; Song, Y.; An, Z.; Zhang, X.; Zhou, X.; Shi, Z.; Sheng, Y.; Zou, H. Novel highly efficient single-component multi-peak emitting aluminosilicate phosphors co-activated with Ce^{3+}, Tb^{3+}

https://doi.org/10.1021/jacsau.2c00568
JACS Au 2022, 2, 2809−2820

and Eu^{2+}: luminescence properties, tunable color, and thermal properties. *Phys. Chem. Chem. Phys.* **2018**, *20*, 1591−1607.
(88) Huang, Y.; Feng, W.; Zhou, Z.; Zheng, H.; Zhao, Y.; Yan, H.; Lü, X. Tetraphenylethylene-based Eu^{3+}-metallopolymers with aggregation-enhanced white emission for self-calibrating temperature sensing and white light-emitting diodes (WLEDs). *J. Mater. Chem. C* **2022**, *10*, 7586−7593.

https://doi.org/10.1021/jacsau.2c00568
JACS Au 2022, 2, 2809−2820